We are IntechOpen,
the world's leading publisher of
Open Access books
Built by scientists, for scientists

4,800

Open access books available

122,000

International authors and editors

135M

Downloads

154

Countries delivered to

Our authors are among the

TOP 1%

most cited scientists

12.2%

Contributors from top 500 universities

CLARIVATE ANALYTICS

BOOK CITATION INDEX

INDEXED

WEB OF SCIENCE™

Selection of our books indexed in the Book Citation Index
in Web of Science™ Core Collection (BKCI)

Interested in publishing with us?
Contact book.department@intechopen.com

Numbers displayed above are based on latest data collected.
For more information visit www.intechopen.com

Methodology of Designing Power Converters for Fuel Cell Based Systems: A Resonant Approach

Maria Teresa Outeiro and Adriano Carvalho

Additional information is available at the end of the chapter

http://dx.doi.org/10.5772/54674

1. Introduction

There has been an increased interest in the use of renewable energy sources, which is due to the limitations in fossil fuel reserves and to planet pollution. The research in the new sources of energy, such as photovoltaic, wind and fuel cells can be used to enhance the safety, reliability and sustainability of the planet, because they are environmentally friendly, highly efficient and renewable cycles. Particularly fuel cells appear in this context as an attractive power source because they generate electricity from hydrogen through an electrochemical process, which is virtually free of emissions and noise and only water and heat are the by-products. In addition, they present several advantages such as: silent, high potential for cogeneration applications, adaptable to a wide range of power and applications.

In this context, the chapter main goal is the analysis design and implementation of power generation systems based on fuel cells, which demands to careful selection of both; i) the fuel cell model and ii) the power electronic converter.

Then, the first part of the chapter presents and characterizes a semi-empirical model of the PEM fuel cell, including its static and dynamic behaviours and thorough some experimental tests made with the commercial system Mark 1020 constraints imposed by the PEM to the converter are established, regardless the topology of the power converter.

The second part of the chapter make considerations on the most suitable topologies of converter for this application type, and considering the requirements imposed by the PEM Mark 1020, a new efficient high power converter topology is selected, designed and implemented experimentally.

The converter follows a resonant approach that provides low component stresses, high frequency operation, soft-switching commutation, and operation under a wide range of input and output conditions.

The control of the converter is divided into two parts, namely: i) the voltage controller, which is responsible for keeping constant the output voltage of the converter under loading variations and ii) the PEM controller, which is responsible for improving the performance by keeping the PEM fuel cell in its optimal operating point.

The results are firstly presented for the PEM fuel cell and then for the whole system with load disturbance.

The results demonstrate that the proposed converter is a good selection to improve the efficiency of PEM fuel cells because it allows an adequate control of the power delivered by the fuel cell while maintaining the requirements imposed by the load and minimizing the losses by using soft-switching control.

2. PEM fuel cell

A PEM fuel cell can be described as a static device that converts the chemical energy of a fuel directly, isothermally, and continuously into electrical energy. In this process, only the reaction between hydrogen and oxygen occur. The only by-products are water and heat. Similarly to a battery, a fuel cell consists of two electrodes (anode and cathode) and an electrolyte. Whereas a storage battery contains all the substances in the electrochemical oxidation-reduction reactions involved and has therefore a limited capacity, the fuel cell is supplied with its reactants externally and operates continuously as long as it is supplied with fuel. The basic scheme for a single cell is represented in Figure 1 and the reactions involved in the anode side, the cathode side and the overall reaction of the process are described by the equations 1 to 3 follows.

$$H_2 \rightarrow 2H^+ + 2e^- \tag{1}$$

$$2H^+ + \frac{1}{2}O_2 + 2e \rightarrow H_2O \tag{2}$$

$$H_2 + \frac{1}{2}O_2 \rightarrow H_2O \tag{3}$$

2.1. Modelling of the PEM fuel cell

Many proton exchange membrane (PEM) fuel cell models have been investigated and presented in the literature [1-12]. The process of selecting the fuel cell model needs to clarify what are the necessary features to take into account in the model [7].
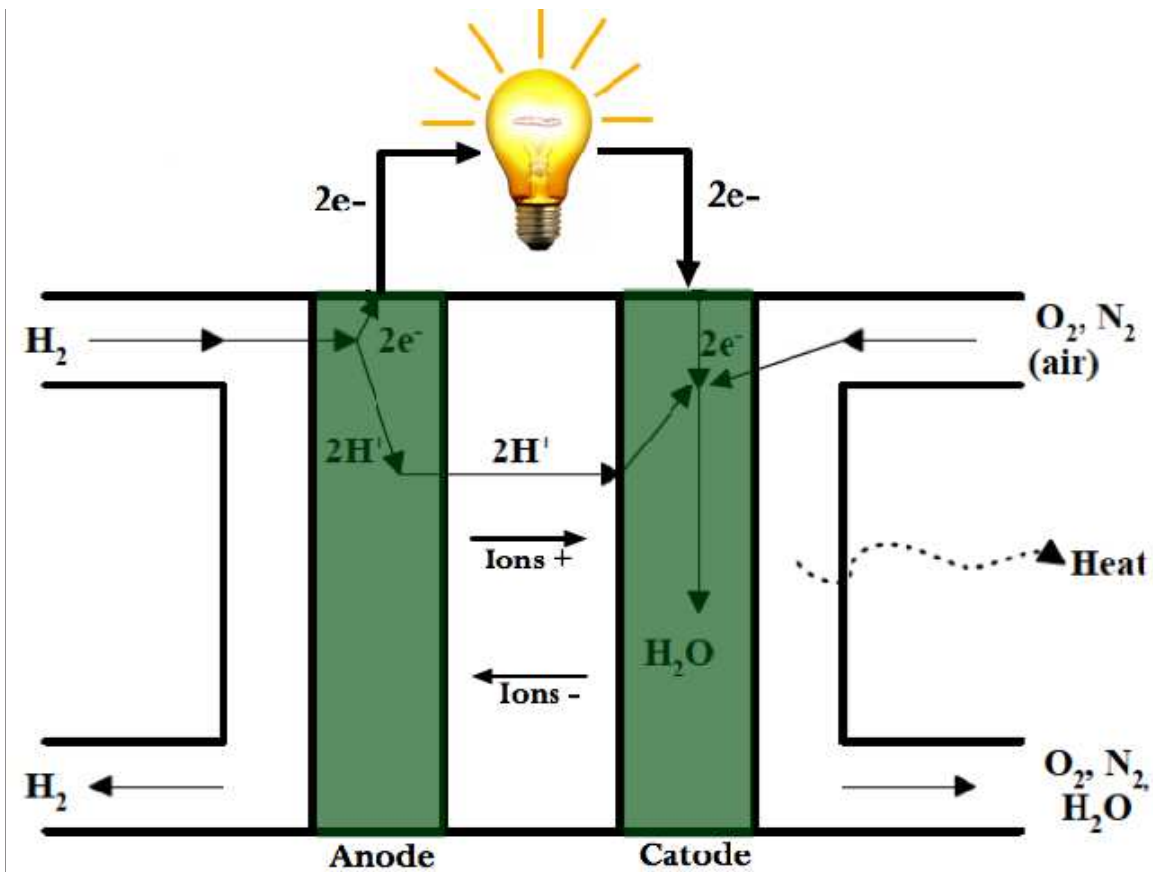
Figure 1. Scheme of a single cell.

The model selection differs for each application and user and the initial decisions are important to avoid changes later in the model evaluation process. The theoretical models are normally detailed, complex and usually require large computation time [8,9,11-12]. The semi-empirical models give a general voltage-current relationship without examining in depth the physical and electrochemical phenomena involved in the operation [1,5,6,10]. These models are usually characterized by simple implementation and faster simulation.

The electrical equivalent circuit represented Figure 2 corresponds to the semi-empirical model adopted for this study. This circuit is the electrical equivalent of the static and dynamic behaviour of the PEM fuel cell and includes the effects of the thermodynamic potential of the fuel cell and the losses. The equations 4 to 9 represent the static behaviour of the PEM while the dynamics is represented by equations 10 and 11. The capacitor C corresponds to the fuel cell phenomenon known as "charge double layer" on which the interface electrode/electrolyte acts as storage of energy element. The electrical power and efficiency are represented by equations 12 and 13 respectively.

Output voltage of one cell:

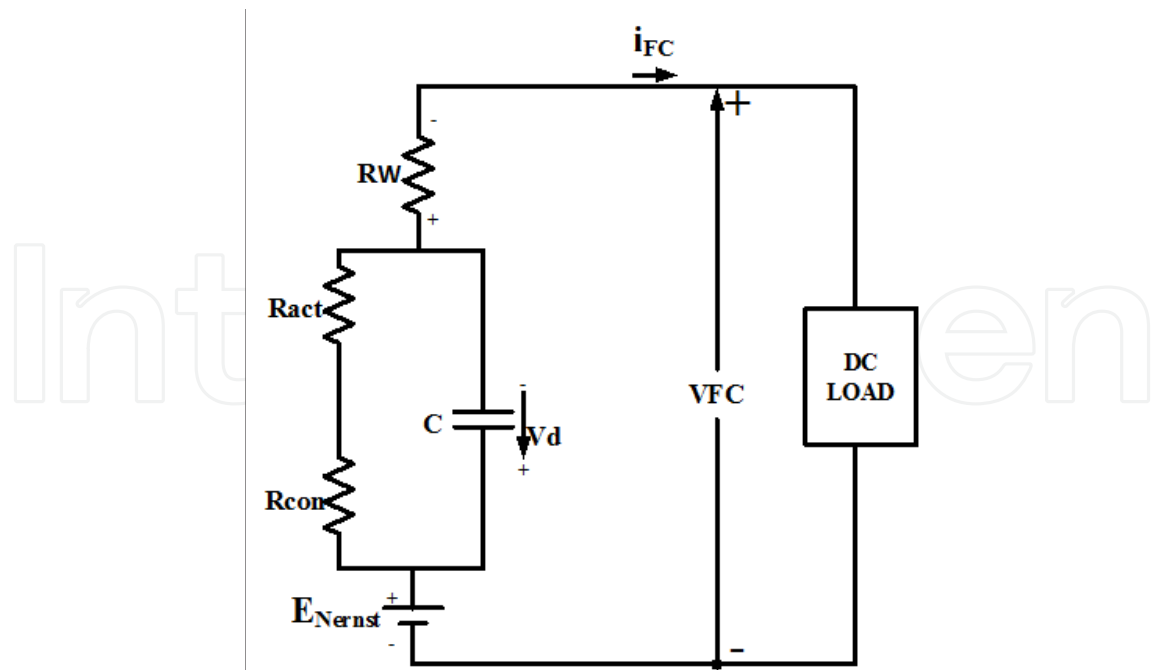$$V_{FC} = E_{Nernst} - V_{act} - V_{Ohmic} - V_{con} \qquad (4)$$

Figure 2. Electrical equivalent circuit of the PEM fuel cell.

Thermodynamic potential:

$$E_{Nernst} = 1.229 - 0.85 \times 10^{-3} \times (T - 298.15) + +4.31 \times 10^{-5} \times T \times \left[\ln(P_{H2}) + \frac{1}{2} \ln(P_{O2}) \right] \qquad (5)$$

Activation over-potential:

$$V_{act} = -\left[\xi 1 + \xi 2 \times T + \xi 3 \times T \times \ln(CO_2) + \xi 4 \times T \times \ln(i_{FC}) \right] \qquad (6)$$

Ohmic over-potential:

$$V_{ohmic} = i_{FC} (R_M + R_C) \qquad (7)$$

Concentration over-potential:

$$V_{con} = -B \times \ln \left(1 - \frac{J}{J_{max}} \right) \qquad (8)$$

Output voltage of the stack:

$$V_s = n \times V_{FC} \qquad (9)$$

Voltage across capacitor:

$$\frac{dV_d}{dt} = \left(\frac{1}{C} \times i_{FC}\right) - \left(\frac{1}{\tau} \times V_d\right)$$ (10)

Electrical Time-constant:

$$\tau = C \times Ra = C \times \left(R_{act} + R_{con}\right) = C \times \left(\frac{V_{act} + V_{con}}{i_{FC}}\right)$$ (11)

Electrical power:

$$P_{FC} = i_{FC} \times V_{FC}$$ (12)

Efficiency:

$$\eta = \mu_f \times \frac{V_{FC}}{1,48} \times 100\%$$ (13)

2.2. Experimental tests made with the PEM Mark 1020

The circuit of Figure 3 corresponds to the experimental setup performed to obtain the electrical PEM characteristics. For each step of load the data is logged when the fuel cell achieved the steady-state operation.
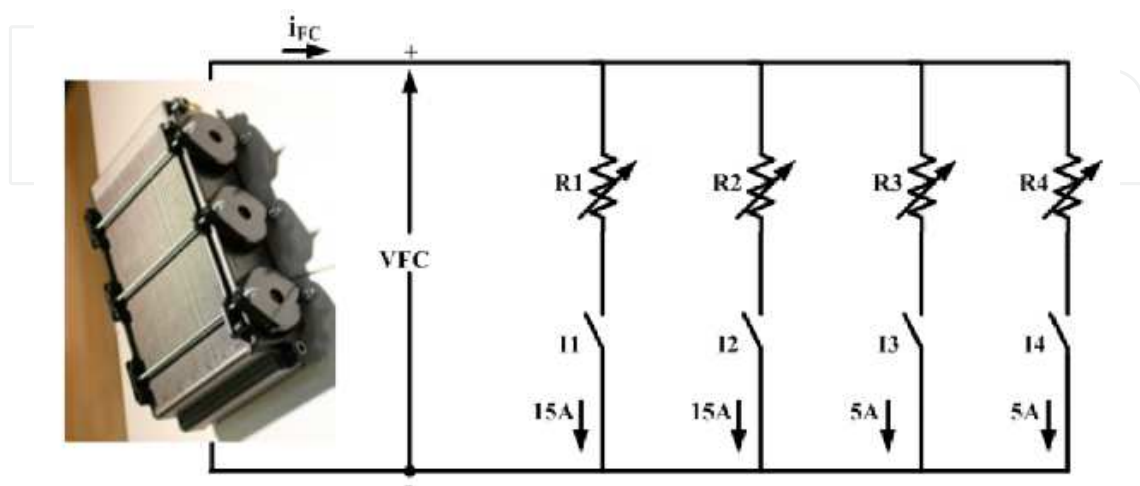
Figure 3. Electrical circuit to test the PEM fuel cell Mark 1020.

2.2.1. Output voltage and power

The output voltage is measured by directly connecting the digital multimetter in parallel with the fuel cell. This is an uncontrolled DC voltage, which fluctuates with the load as well as with changes in the fuel input to the system. Figure 4 shows the stack voltage while Figure 5 corresponds to the stack power of the PEM Mark 1020. The results obtained for the both electrical variables are in accordance with the information provided by the manufacturer of the stack.
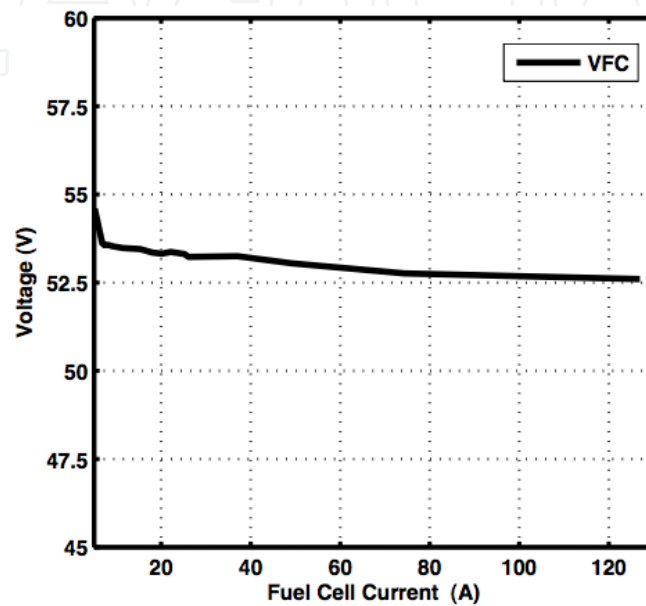

Figure 4. Fuel cell voltage of PEM Mark 1020.
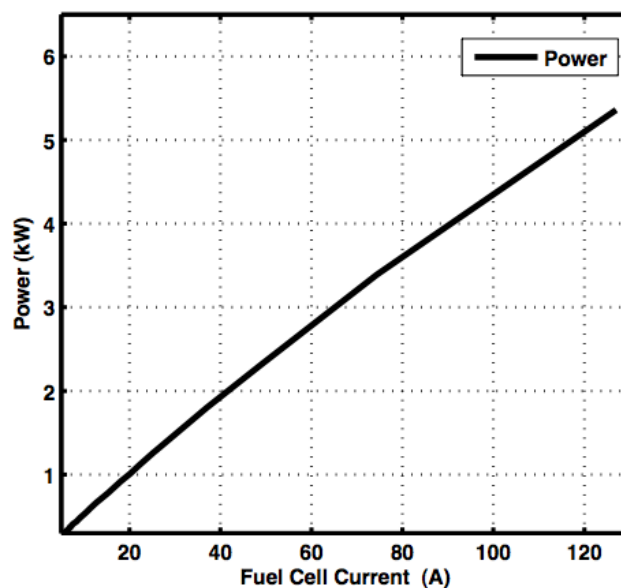
Figure 5. Electrical power of PEM Mark 1020.

2.2.2. Efficiency and hydrogen consumption

The efficiency of PEM Mark 1020 is in the range of 40 % - 55 %, which minimum and maximum values are 45.15 % and 55.49 % respectively. The efficiency decreases slightly with the increase of the current density as is shown in Figure 6. The hydrogen consumed by the stack Mark 1020 is represented in Figure 7 below and is proportional to the power delivered by the fuel cell.
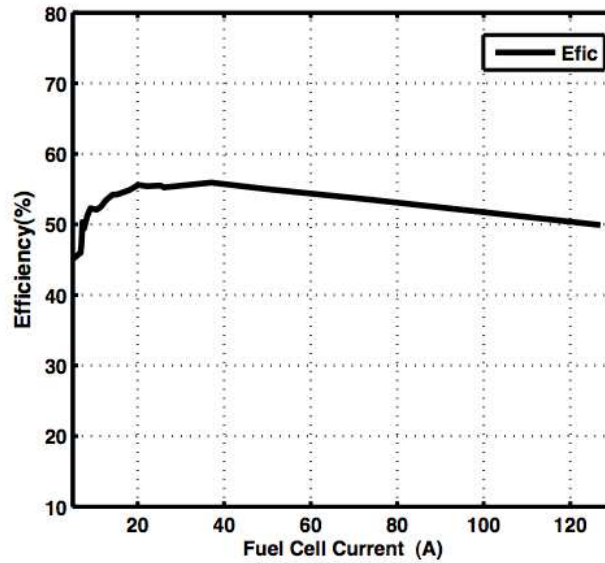

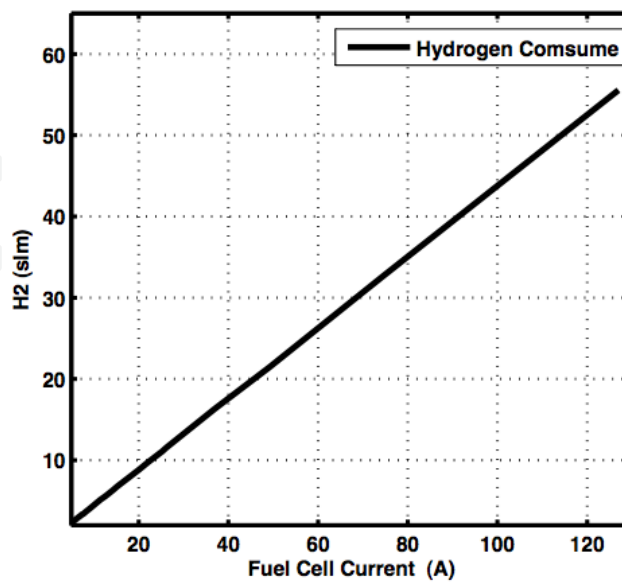**Figure 6.** Figure 6. Efficiency of the PEM Mark 1020.

Figure 7. Hydrogen consumed by the PEM Mark 1020.

2.2.3. Constraints imposed to the converter

Regardless the topology of the converter selected, the constraints imposed by the PEM fuel cell should be respected that is, the minimum and maximum values of the voltage, the current and the power, which for the PEM Mark 1020 are listed in the Table 1 below.

Ifc (A)	Vfc (V)	Power (W)
2.8	23.71	66
24	19.11	492

Table 1. Constraints imposed to the power system by PEM MARK 1020.

3. Power electronic converters for PEM fuel cells

Power electronic converters are used in fuel cell systems to convert the DC electrical power generated by the fuel cell into usable AC or DC power through power electronic circuits. The power electronic converter plays an important role on the interface of the fuel cell system as power generating system and many solutions are already presented in the literature [14-30]. The output voltage of the fuel cell varies normally in the range of 20 V to 50 V and the possible converter topologies that can be used are such as; DC-DC together with DC-AC, DC-AC interfacing directly the fuel cell to the grid, or DC-DC together with AC-AC isolated by a transformer.

Figure 8 shows that the DC-DC power converters can be divided according to the operation mode into tree types: 1) the linear mode, 2) the switching mode and 3) the soft switching or resonant mode. The main difference between them is caused by efficiency. The soft-switching or resonant has some advantages compared to the linear like; the high switching frequency, which enables the use of a small ferrite transformer core, it may operate in a much larger DC input voltage range than the linear regulators, and it often has a higher efficiency. However, there are some drawbacks associated too, the noise at the supply may be increased according to different power switching techniques, and the control circuitry is more complicated compared to the linear one. Figure 8 also shows that the switching-mode topologies are divided into two types, the isolated and the non-isolated. Non-isolated DC-DC converter topologies are the Buck, Boost and Buck-Boost converters; and further, the Cuk converter. For many applications, isolation between the input and the output is a necessary requirement within the converter. By inserting isolation transformers into the four basic non-isolated switching topologies presented above, four single-ended isolated switching DC-DC converters can be obtained, namely; Forward, Boost, Flyback and Cuk converters. Nonetheless, the single switch topology is not an ideal solution for higher power converters, since these converters need a higher power trans-

former. Therefore, another group of DC -DC isolated converters utilizing more than one switch are identified: Push-pull, Half-bridge and Full-bridge converters.
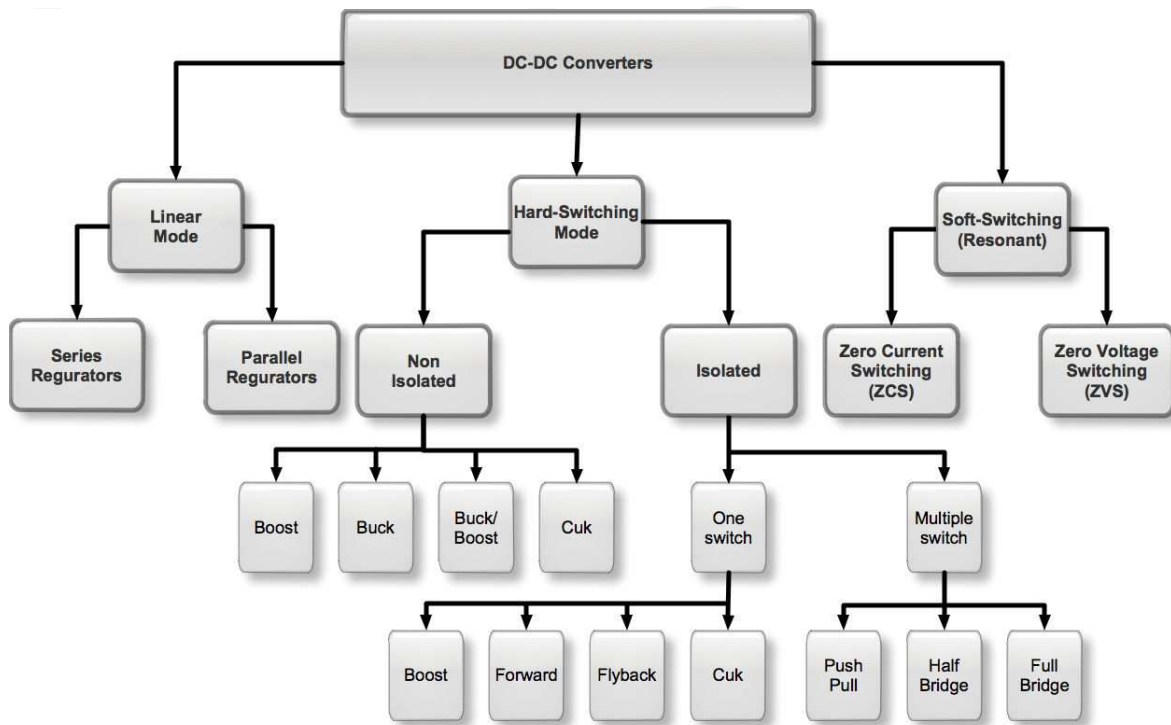

Figure 8. DC-DC power converter family tree.

In switched-mode topologies, finite duration of the switching transitions will cause high peak pulse power dissipation in the devices, degradation of the converter efficiency and, also can lead to transistor damage during the turn-off transition. Employing load-line snubbers can reduce this problem. When using snubbers the stress of the switches are minimised, as shown in Figure 9. However, with the appearance of new power electronic converters based on soft-switching technologies, [15,17,19,20-22,30], the reduction of switching losses and the continual improvement of power switches allow at being able to increase the switching frequency. In this type of converter the turning on and turning off of the converter switches appears when the switch voltage or the switch current is zero, as shown in Figure 9 [23].
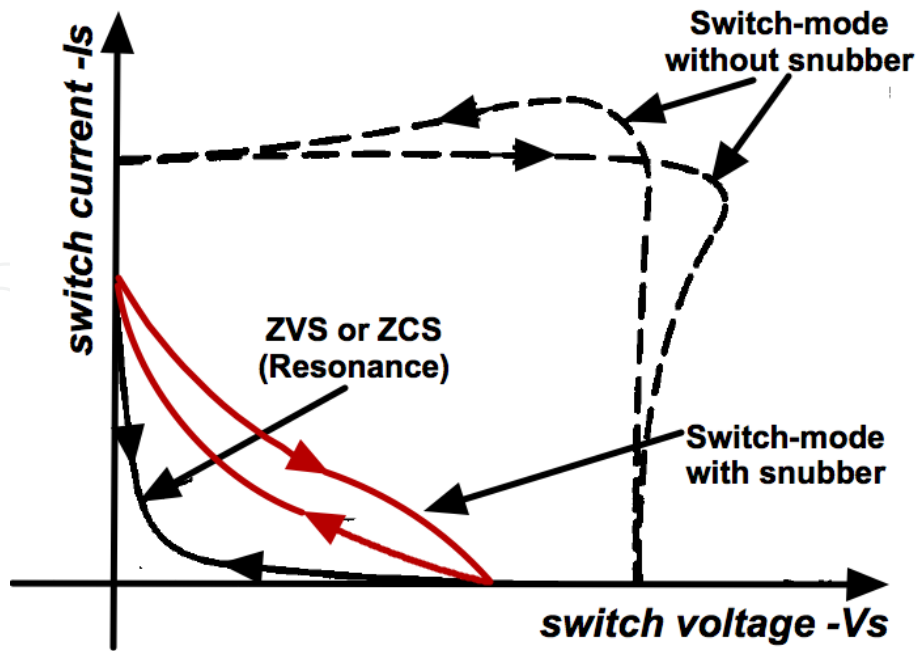
Figure 9. Switching loci trajectories of the different converter types.

Figure 10 provides an arrangement for a soft-switching resonant converter. An inductor -Ls and a capacitor-Cs have been added to help the switch action. A similar *LdC*d pair is added to the diode. In any of these soft switching cases, switch action at a zero crossing cuts off the ringing resonant waveform. This technique is often called quasi-resonance.
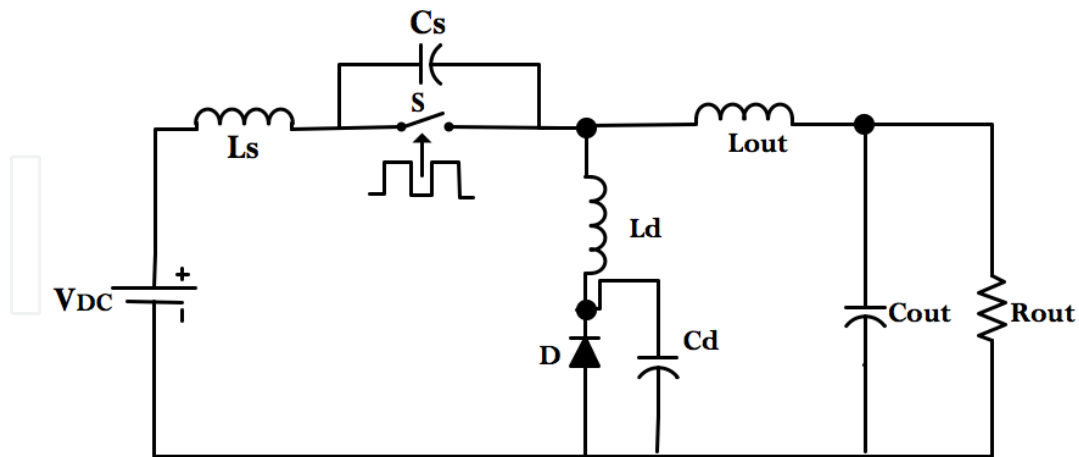

Figure 10. General structure of a resonant converter, where ZVS or ZCS can be obtained.

To create conditions for the ZCS or ZVS in DC-DC converters, the resonance or soft switching approach can be used. The ZVS or ZCS can be obtained by re-arranging the resonant component Figure 10, whose combinations offer several possibilities for resonant action as follows:

1. If the parts are chosen so that Cs and Ld are very small and have minimal effect on the circuit action. With Ls and Cd forming an LC series combination, the transistor operation can take advantages of current zero crossing for ZCS.

2. If the values of Cs and Ld are small, then the transistor supports ZVS [24].

3. It is also possible to use all four parts to support ZVS and ZCS action together, called multi-resonance, but this is not a common technique.

ZCS topologies can eliminate the switching losses at turn-off and reduce the switching losses at turn-on. If a relatively large capacitor is connected across the output diode during resonance, the converter operation becomes insensitive to the diode's junction capacitance. The major limitations associated with ZCS when Mosfet's are used are the capacitive turn-on losses. Thus, the switching loss is proportional to the switching frequency, during turn-on, considerable rate of change of voltage can be coupled to the gate drive circuit through the Miller capacitor, thus increasing switching loss and noise. Another limitation is that the switches are under high current stress, resulting in high conduction loss. ZVS eliminates the capacitive turn-on loss. It is suitable for high-frequency operation. For single-ended configuration, the switches could suffer from excessive voltage stress, which is proportional to the load. The output regulation of the ZCS and ZVS resonant converters can be achieved using variable frequency control. The ZCS [20-22] operates with constant on-time control, while ZVS [24] operates with constant off-time control.

3.1. Requirements for selecting the converter topology

For the selection of the converter topology the following requirements are considered in order to ensure the maximum efficiency and minimum cost of the power generation system.

1. Control of output voltage according to a given reference;

2. Deliver current with little ripple and harmonic contend

3. High efficiency in the whole operating range

4. Properly operation in all conditions

5. Incorporated filtering and storing possibilities

A comparative analysis of the major topologies of DC-DC converters described above is presented below.

3.2. DC-DC converter topologies

Power electronic converters in general and DC-DC converters in particular have a great importance on the performance and efficiency of energy production process based on fuel cells. The control of the operation point of the fuel cell requires appropriate use of static power converters, capable of providing accurate support to the control methods. The main objective to be achieved when applying the converters to fuel cells is obtaining the maximum efficiency using the most appropriate control strategies, taking into account requirements described above. As

described above, different converter topologies can be used as represented in figures 11 to 13 below. Usually the DC-DC converter is put between the fuel cell and the inverter, which performs two functions, namely; 1) acts as DC isolation for the inverter; and 2) produces sufficient voltage for the inverter input so that the required magnitude of the AC voltage can be produced. The inverter can be single-phase or three-phase depending on the utility connection.
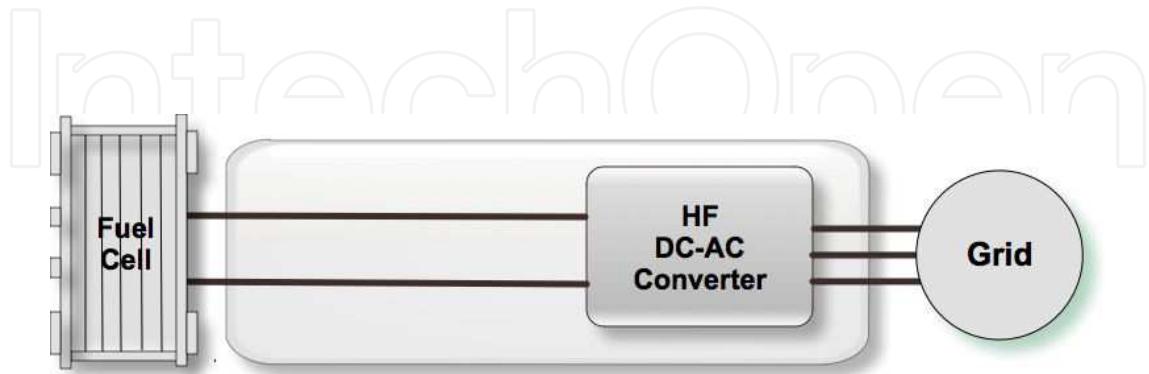

Figure 11. Configuration of a DC-AC converter interfaced directly to the grid.
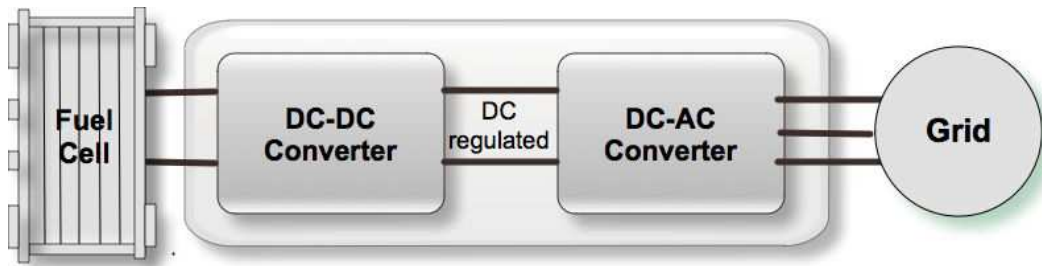
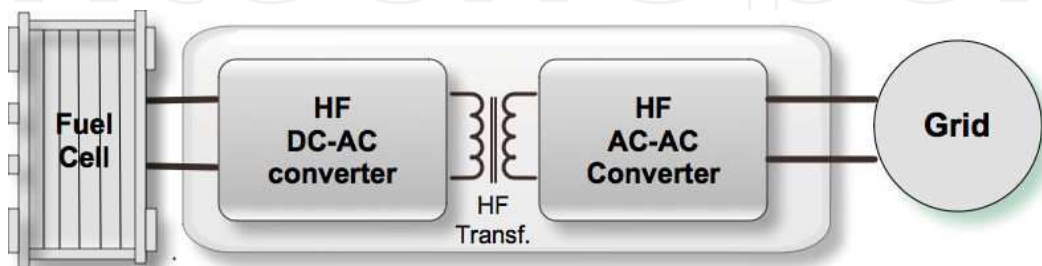**Figure 12.** Configuration of a DC-DC followed by a DC-AC converter interfacing the grid.

Figure 13. Configuration of a DC-AC followed by a AC-AC converter interfacing the grid.

3.2.1. Series resonant converter with capacitive output filter

The converter topology shown in Figure 14 is in conformity with the considerations presented above. This is a modified series resonant converter (SRC), which uses an (L-C)||L resonant tank for soft switching of HF switches. The main characteristics of such type of converter can be summarized as follows:

1. This configuration gives high efficiency at all varying load and line conditions but it decreases with increase in input voltage.

2. The full range ZVS (full load to light load) is achieved.

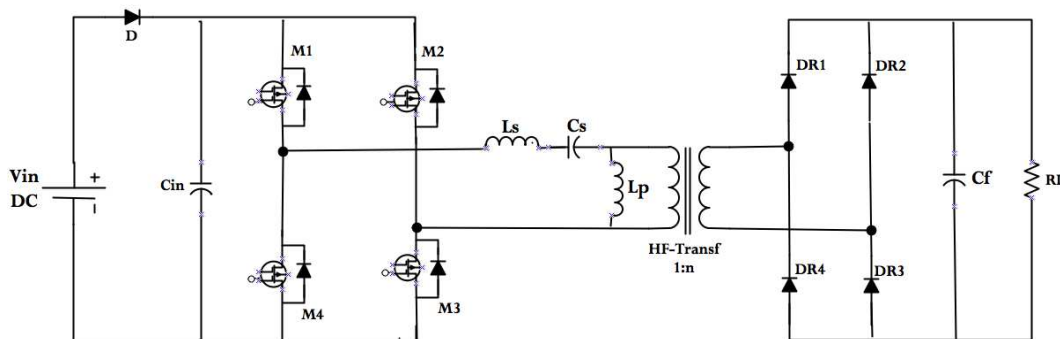3. Switch peak current reduces with load but increases significantly with change in input voltage.

Figure 14. Series Resonant converter with capacitive output filter.

3.2.2. Series resonant converter with inductive output filter

The converter topology shown in Figure 15 is an LCL type SRC with inductive output filter. This uses an LCL resonant tank for soft switching of high frequency switches and an inductive output filter. Its main characteristics can be summarized as follows:

1. The full range ZVS (full load to light load) is achieved.

2. Rectifier diode voltage rating is higher, but with application of ultra fast recovery diodes of high voltage rating with low forward voltage drop does not affect the efficiency much.

Note: This configuration can also be modified to a series resonant converter (SRC), which uses an (L-C)||C resonant tank for soft switching of high frequency switches, which, in this case is also called series-parallel resonant converter (SPRC).
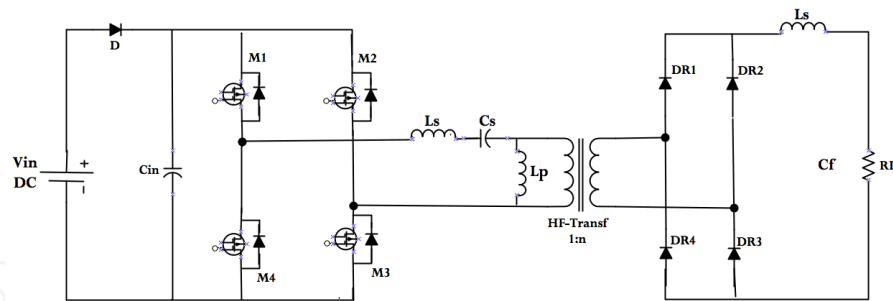
Figure 15. Series Resonant converter with inductive output filter.

3.2.3. PWM full-bridge converter with inductive output filter

The configuration shown in Figure 16 is Phase-shifted full bridge converter with inductive output filter. This is most widely used soft-switched configuration for high power applications. This constant frequency converter features ZVS of the primary switches with relatively small circulating circuit. The ZVS is achieved by filter inductance, transformer leakage inductance, snubber capacitance and parasitic junction capacitances of switches. The control of the output voltage at constant frequency is achieved by phase shift technique. Its main characteristics can be summarized as follows:

1. The major limitation of this configuration is loss of duty cycle on the secondary side.

2. High voltage stress on rectifier diodes on secondary side.

3. Parasitic ringing at the secondary side of transformer.

4. Large inductor may increase ZVS range but needs a transformer turns-ratio (Np/Ns) to be decreased at the same time, which increases primary side current, causing large conduction losses, which decreases converter efficiency.

5. A good compromise between the transformer turns-ratio and leakage inductance is required to keep conduction losses lower.
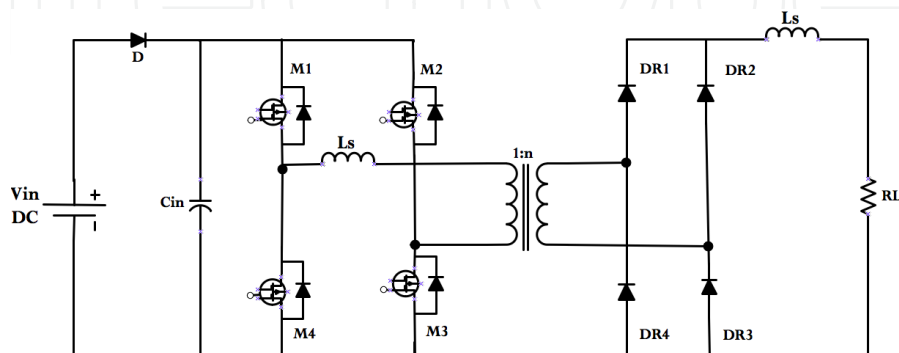

Figure 16. PWM full-bridge converter.

3.2.4. Full-bridge converter with controlled at secondary side

The configuration shown in Figure 17 corresponds to a secondary side controlled converter with a full-bridge inverter on primary side and phase-controlled rectifier on secondary side. The switches on primary side are operated by complementary gating scheme with fixed duty ratio. The switches on secondary side are controlled to produce phase difference between primary and secondary side voltages of HF transformer to control the output voltage with load and input line voltage variations.

The main characteristics of this configuration can be summarized as follows:

1.   Control is easy and simple.

2.   The switches on secondary side show ZVS or ZCS depending upon the line and load, which represents a drawback of the converter.

3.   The switches on secondary side show ZVS for lower input voltage and ZCS for higher input voltage conditions.

4.   The efficiency of this converter is near to 92%, obtained at full load and varying line voltage.
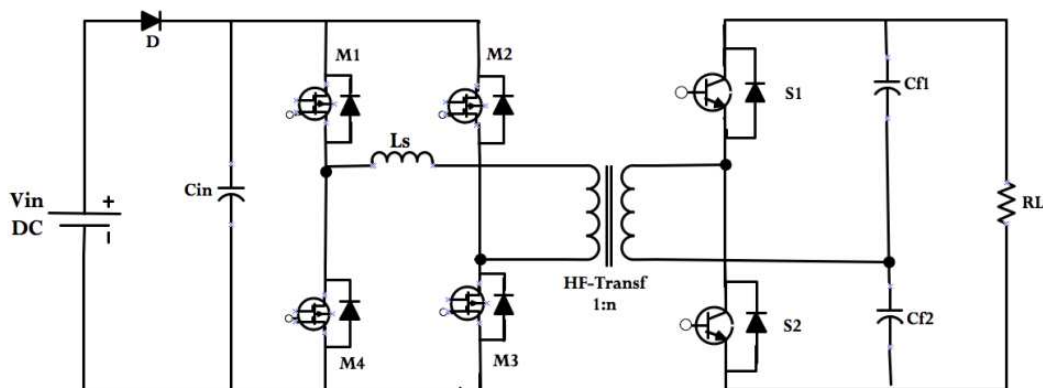

Figure 17. PWM full-bridge converter.

3.2.5. Current-fed two-inductor boost converter

Figure 18 shows the current-fed two-inductor boost converter, which is a dual of voltage-fed half-bridge converter configuration. This topology requires a very small turns ratio transformer with only two switches used on the primary side. The turn off of the primary switches is smooth since voltage across the switches is sinusoidal. Also the same for turn on and turn off of rectifier diodes. However, the peak and average current through rectifier diodes is high and this is very difficult to achieve ZVS at variable line input and load condition. This topology is a good selection for constant-input and constant-output voltage applications.
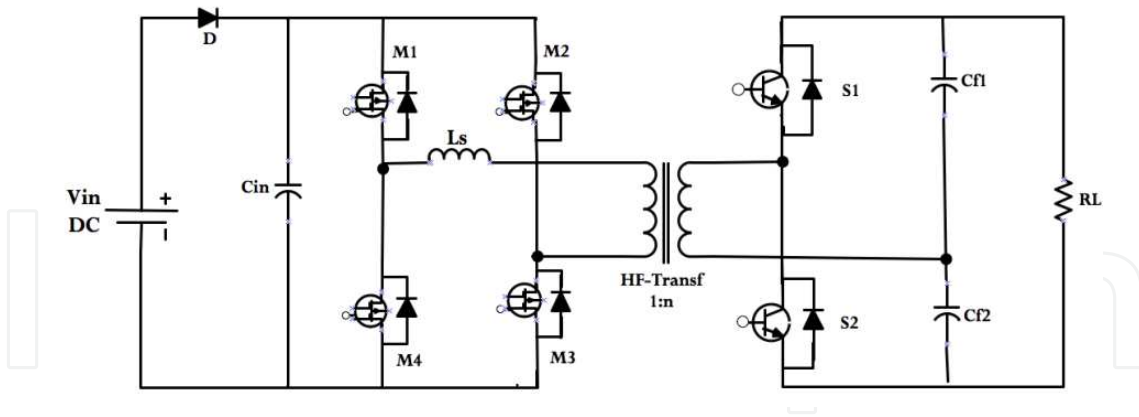
Figure 18. Current-fed two-inductor boost converter.

3.2.6. Bidirectional current–fed converter

The configuration of Figure 19 corresponds to a soft-switched bidirectional current-fed boost converter. The active switches in the both sides of the transformer make this converter bidirectional. Normally the Mosfets are used in the low voltage side and the IGBTs are used in the high voltage side. This configuration can be in push-pull, half-bridge or full-bridge, with the full-bridge considered one of the best topology choices for fuel cell applications.
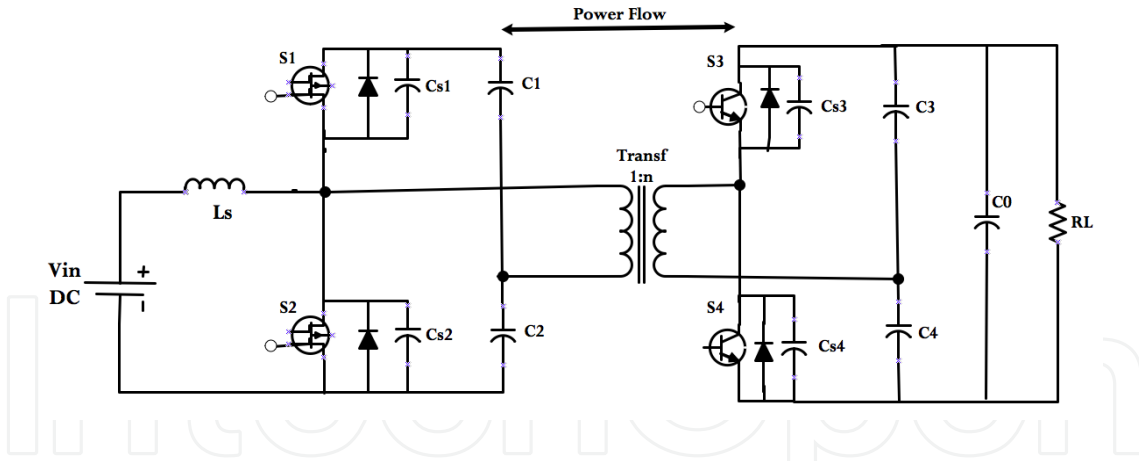

Figure 19. Soft-switched bidirectional current-fed boost converter.

3.3. Selection of converter topology and operation

Considering the analysis made previously a full-bridge series-resonant inverter, followed by a high frequency transformer and a rectifier, composes the topology selected. Additionally, two low-pass filters are included, one in the primary side which is used to protect the PEM of high ripple-current and another in the secondary side, to improve the quality of the energy supplied by the power system to the load or the grid. Figure 20 below represents electrical scheme of its topology, which is also called a series resonant converter (SRC).
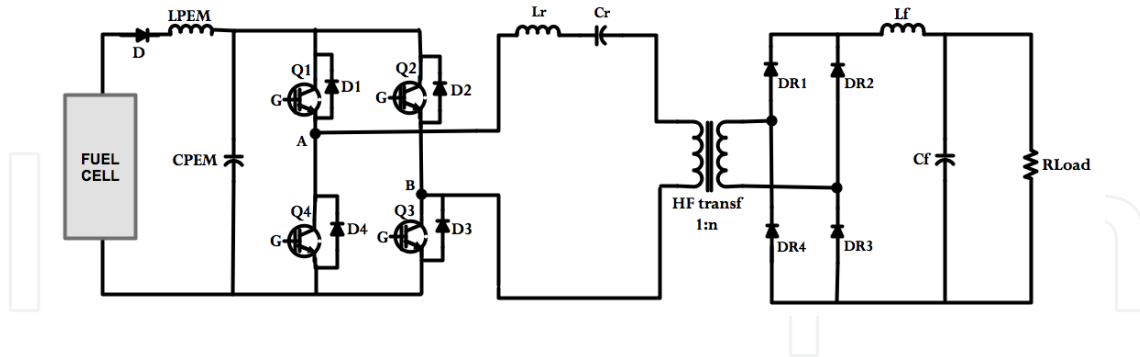
Figure 20. Electrical circuit of the SRC.

The operation of the converter can be described as follows: the voltage supplied by the fuel cell stack, which is typically low must be converted to a high and constant level, for example; 48 V or 400 V_{DC} in order to be able to feed an electric vehicle or to be sent to the grid through an inverter. The HF transformer is a step-up voltage transformer, which also serves as galvanic isolation between the high and low voltage levels of the circuits. The waveforms of the voltage and current in the LC series resonant circuit in the primary side of the transformer are sinusoidal. Selecting appropriate values for the Lr and Cr components, the resonant frequency of the circuit is established. Then, the DC voltage of the fuel cell is firstly inverted in the primary side of the HF transformer, being rectified on the secondary side. The low pass filter in the primary side (L_{PEM}, C_{PEM}) allows at protecting the PEM fuel cell from the ripple current and voltage produced by the converter, and also allows the storage of energy in the DC bus. The low pass filter in the secondary (L_f, C_f) allows at reducing the ripples of current and voltage to the load, respectively.

3.4. Mathematical analysis of the series resonant converter (SRC)

The series-resonant inverter as part of the topology of Figure 21 is constitute by a controlled full-bridge and a series resonant circuit with natural frequency f_r and impedance Z_r.

The analysis of this circuit by sinusoidal approximation neglects the harmonics of the switching frequency and the tank waveforms, namely the capacitor voltage, V_C and the inductance current, i_L are assumed to be purely sinusoidal.

3.4.1. Voltage

In Figure 21 the output voltage of the full-bridge inverter, which in turn is the input voltage of the series resonant circuit, is a square-waveform, wherein in the first half period [0-π] the IGBTs Q1 and Q3 conduct, while in the second half period conduct IGBTs Q2 and Q4 [π - 2π] as represented by Figure 22 and equation 14.
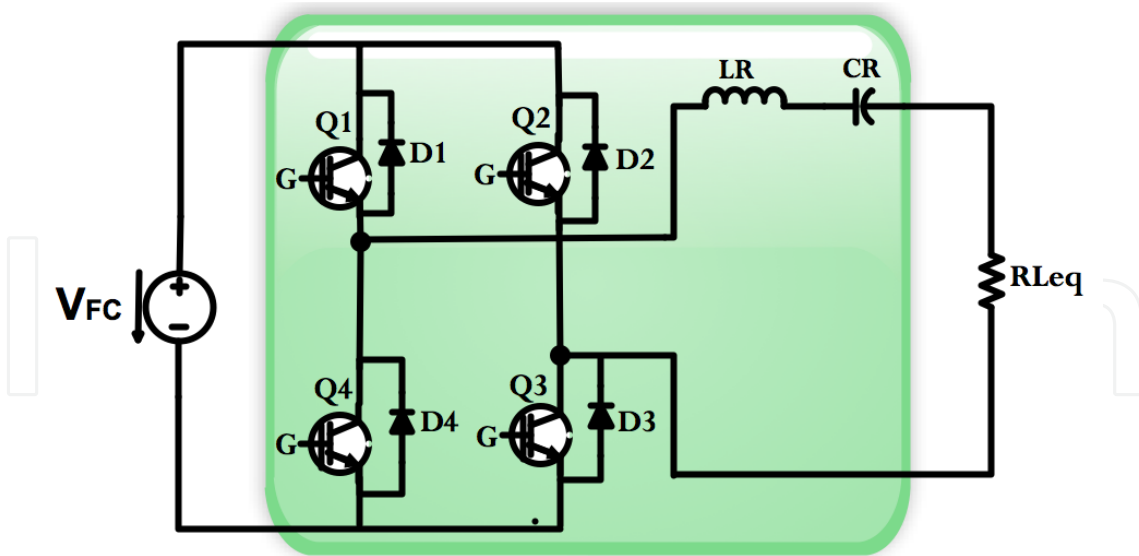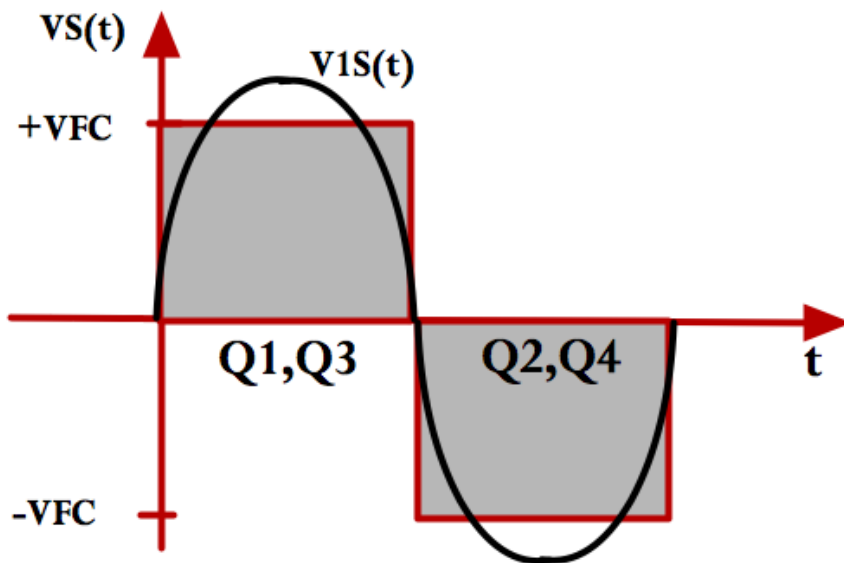
Figure 21. Electrical equivalent circuit of the SRC.

Figure 22. Output voltage in a full-bridge inverter.

$$\begin{cases} +V_{Fc}, \text{ for } 0 < \text{wt} \le \pi \\ -V_{Fc}, \text{ for } \pi < \text{wt} \le 2\pi \end{cases} \tag{14}$$

3.4.2. Current

The current is (t) is equal to the output current +is (t) in the first half period [0-π], and is its inverse -is (t), in the second half period [π - 2π]. Under the conditions described above, the

tank rings sinusoidal and is(t) is well approximated by a sinusoid waveform as represented by the equations 15 and 16.

$$iQ1 = iQ3 = \begin{cases} +\text{Im}\,ax \times \sin(wt - \Phi), & \text{for } 0 < wt < \pi \\ 0, & \text{for } \pi < wt < 2\pi \end{cases} \tag{15}$$

$$iQ2 = iQ4 = \begin{cases} 0, & \text{for } 0 < wt < \pi \\ -\text{Im}\,ax \times \sin(wt - \Phi), & \text{for } \pi < wt < 2\pi \end{cases} \tag{16}$$

A simple equivalent circuit similar to that represented in Figure 23, whose operation can be analyzed by a second-order differential equation as follows, can perform the analysis of the SRC.
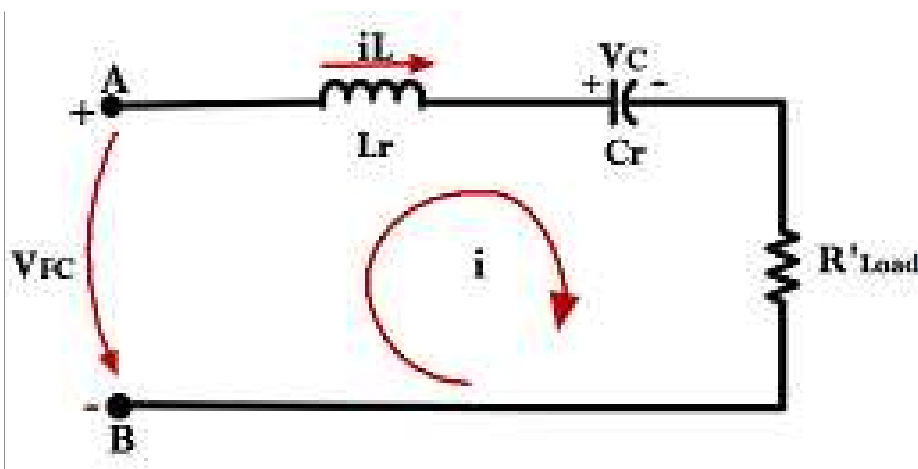

Figure 23. Series resonant circuit with a resistive load.

Applying the Kirchoff loop equation (sum of voltages around loop equals zero), to the RLC circuit of Figure 23 the equation of the series resonant circuit is the follow.

$$Lr\frac{diLr}{dt} + VCr + RI = \bar{V} \tag{17}$$

And the input impedance Z of this circuit is expressed by equation 18 with $R = Z\cos(\theta)$ and $X = Z\sin(\theta)$.

$$\bar{Z} = R + j\left(w\, L_r - \frac{1}{wCr} \right) \tag{18}$$

3.4.3. Angular frequency and reactance

If the reactance of the resonant circuit becomes zero with $XL_r = XC_r$ then Z=R and the circuit operates at resonant conditions that is, for $f_s = f_r$. This is characterized by the angular frequency w_r and characteristic impedance Z_r as defined by equations 19 and 20 follow.

$$w_r = 2\pi f_r = \frac{1}{L_r C_r} \tag{19}$$

$$Z_r = \sqrt{\frac{L_r}{C_r}} \tag{20}$$

3.4.4. Quality factor

The quality factor Q measures the "goodness" or the quality of the circuit. This is the ratio between the power stored in the reactance and the power dissipated in the resistance of the resonant circuit. The quality factor Q, can be defined expressed by the equation 21 or equivalently by equation 22.

$$Q = \frac{w_r \times Lr}{R} = \frac{1}{w_r \times C_r \times R} = \frac{Z_r}{R} \tag{21}$$

$$Q = \frac{1}{R} \times \sqrt{\frac{L_r}{C_r}} \tag{22}$$

3.4.5. Normalized amplitudes of the current and power

Normalized amplitudes of the current and output power in the series resonant circuit as a function of fs/fr and R/Zr =1/Q are represented in figures 24 and 25, respectively. The maximum current value in the circuit occurs at the resonance frequency and with low load resistance. It is also observed that at resonant frequency fr if the load R→ 0Ω then the peak current I→∝ and the system can de destroyed. This analysis leads to the conclusion that it can't ever work with a short circuit in the load side. The maximum output power occurs at the resonance frequency and with low load resistance.
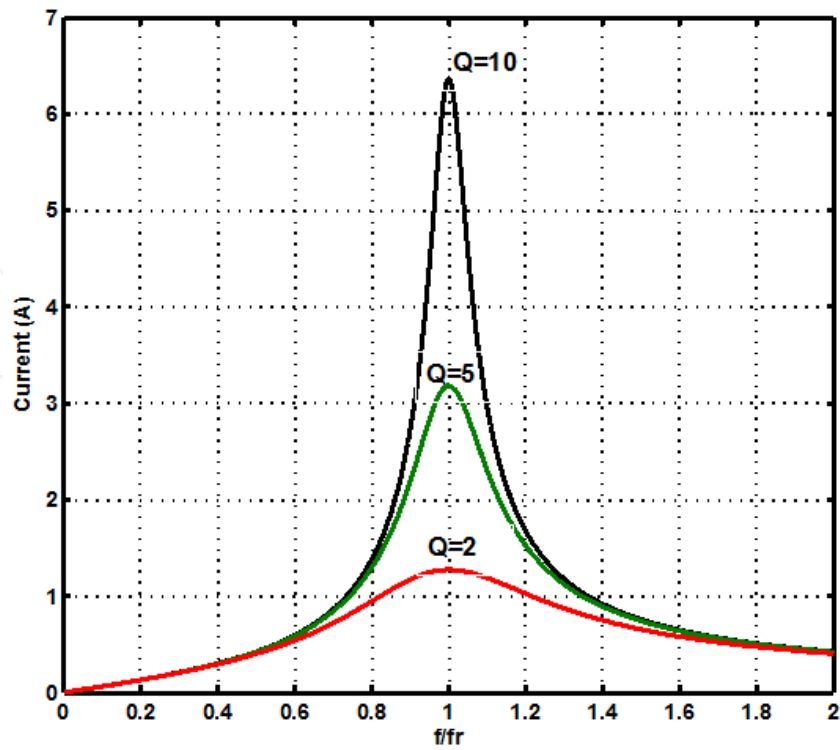
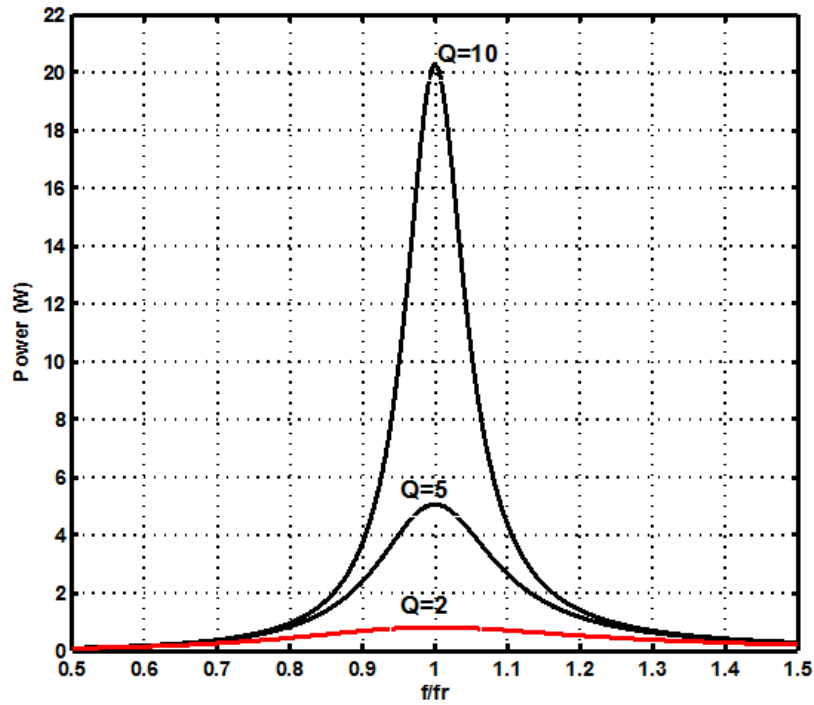**Figure 24.** Amplitude of the current in the series resonant circuit

Figure 25. Amplitude of the power in the series resonant circuit

4. Control

The control consists of two loops; the loop of the voltage or the fast loop and the loop of he PEM or the slow loop. The voltage controller is responsible of controlling the output voltage of the converter, keeping this in a constant value defined by the user even for load variations. The PEM controller is responsible of controlling the operation of the PEM, keeping it in its optimal point that is, producing the electrical power requested by the load with a minimum current and consequently with a minimum of hydrogen consumption. The control structure of the converter as described is represented in Figure 26.
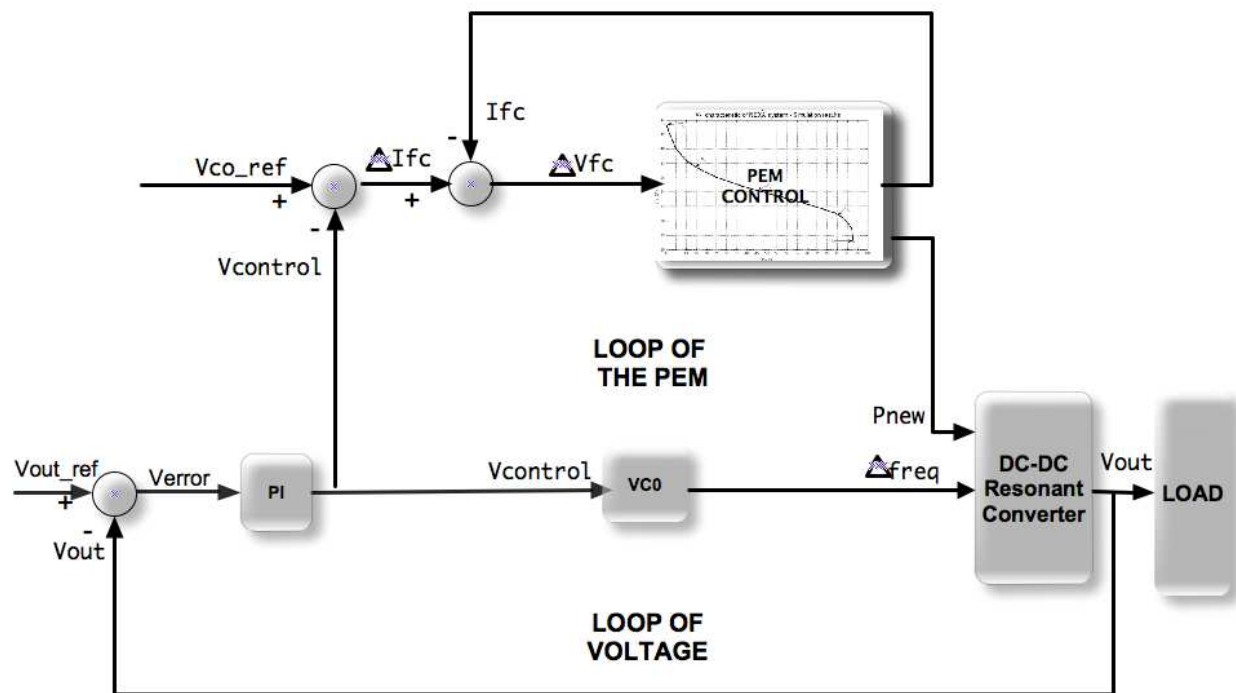

Figure 26. Control structure of the SRC.

5. Experimental setup and results

The experimental setup is represented in Figure 27. It is used to test the all system composed by the PEM Mark 1020, the SRC and the load. The load is composed by a set of several resistors connected in series, whose variation is performed by a manual switch. The fuel pressure that provides a PEM stack is monitored by a standard dial pressure gauge, which maintains it constant in the range of 0.3 to 0.5bar. The ventilator is used to inject the oxidant flow necessary into the stack in order to produce the electrochemical reaction. The voltage of 26.06V represented by the multimetter corresponds to the open-circuit voltage of the PEM.

The experimental results corresponding to the output voltage and current, the PI controller and the resonant current, are presented in this section to validate experimentally the SRC in its stability and dynamics.

Figure 27. Experimental setup of the system.

5.1. Output voltage and current

Figure 28 below allows validating the stability of the voltage control loop of the converter that is, it can be seen that the output voltage, vout remains constant despite variations in the output current that is, in the load. This condition is valid to both situations namelly, the step-up of load corresponding to Figure 28 a) and the step-down of load corresponding to Figure 28 b).
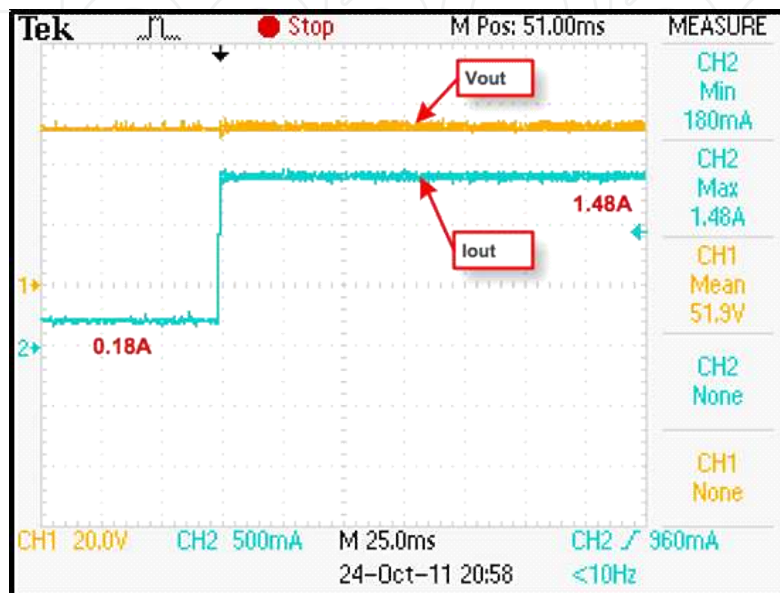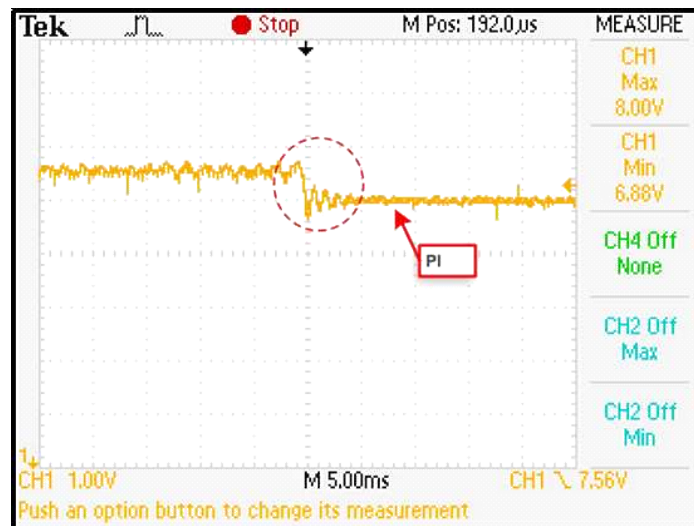

(a) Step-up load condition.
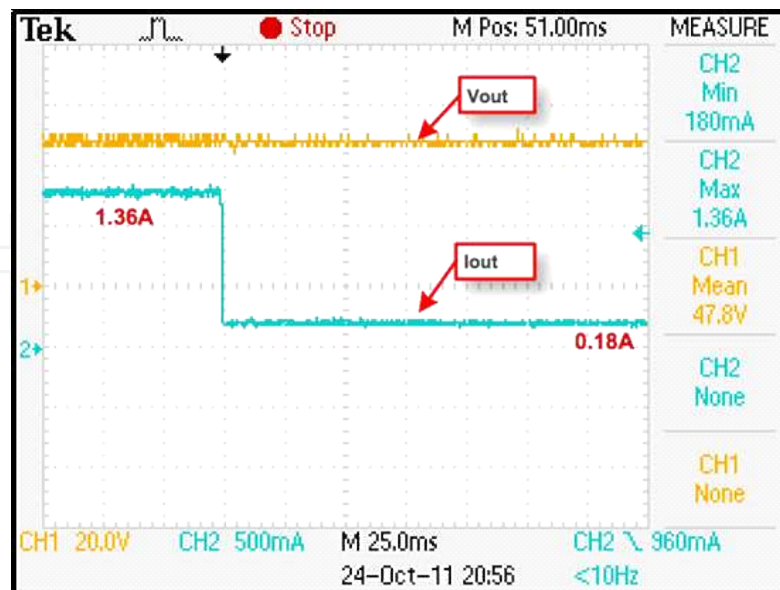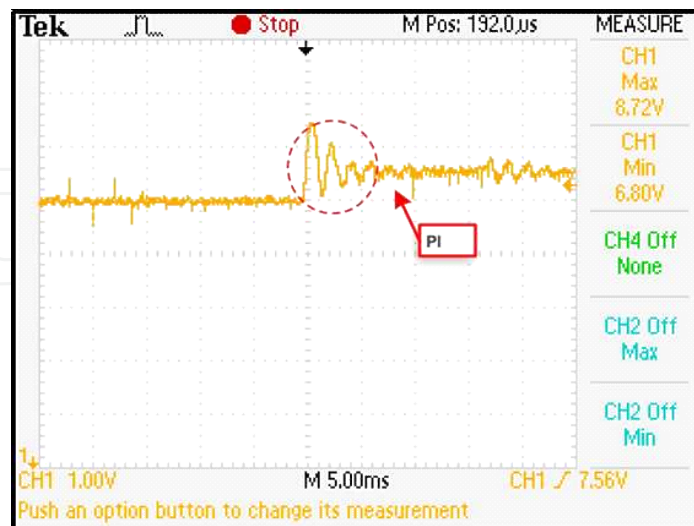

(b) Step-down load condition.

Figure 28. Output voltage (Vout) and current (Iout).

5.2. Proportional integral control (PI)

The dynamics of the system can be evaluated by the analysis of the PI control signal. So, once considered both situations of load variation it appears that the stabilization time of the PI controller is approximately 7ms. In addition it presents a small oscillation which proves that the parameters of the PI control are well adapted to the system Figure 29 a) corresponds to the situation of a step-up load condition while Figure 29 b) corresponds to a step-down of load condition. The error of voltage is given by INA101 such as; $\varepsilon = V_{measured} - V_{reference}$ and accordingly, the objective of the PI controller is to minimize this error for any load variation, as is shown in the two figures below.
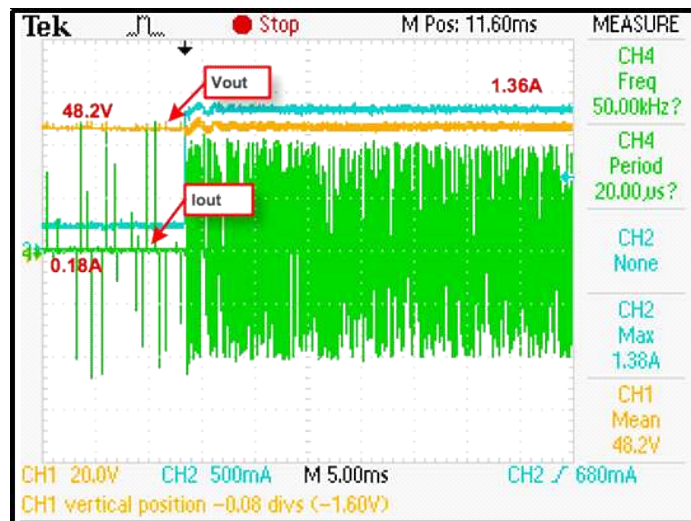

(a) Step-up load condition.
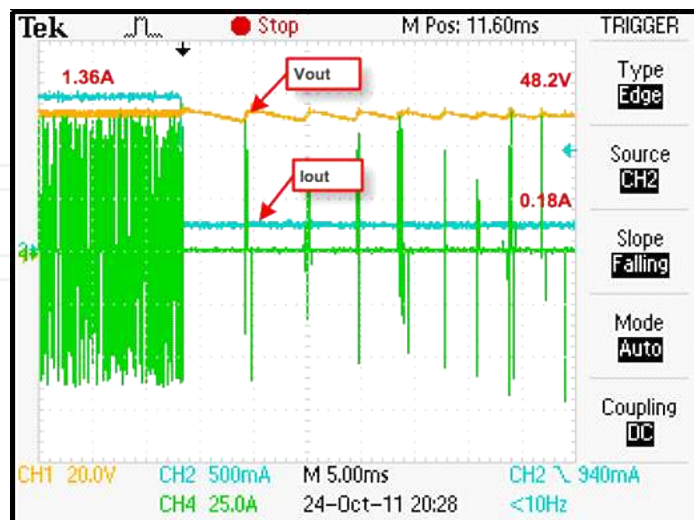

(b) Step-down load condition.

Figure 29. PI Control.

5.3. Resonant circuit operation

Figure 30 corresponds to step-up and step-down load conditions. From its analysis it follows that the converter reacts to the load variation, varying its frequency of operation. Thus, for a small load level (Imin, Rmax) the frequency is low while for a high load (Imax, Rmin) the frequency is high. In dynamic terms it can be seen that the transition in the frequency of operation is instantaneous, hence, we conclude that the system has good dynamic characteristics. It can be also observed that in any of the load variations the output voltage Vout remains constant. This analysis validates the objective defined to the controller, that is it ensures a constant output voltage in order to satisfy the requirements imposed by the power system applications.

(a) Step-up load condition.

(b) Step-down load condition.

Figure 30. Output voltage and current and resonant circuit operation

6. Conclusions

The main objective of the chapter is to discuss the design and implementation of a power generation system based on fuel cells. Accordingly, a methodology of designing and implementing an efficient high power converter system is presented. Moreover the chapter presents also an electrical equivalent model of the PEM fuel cell, which was validated by experimental tests made with the commercial system MARK 1020.

Authors make considerations on the most suitable topologies of converters for this application type, and satisfying several criterions a series-resonant converter topology is selected, whose principle is based on soft-switching methodology. In this context the design and implementation of the converter consisting of a input filter followed by the full-bridge inverter and the series resonant circuit on the primary side and a diode rectifier and output filter on the secondary side was based on the exploitation of their benefits as compared to other types of converters, namely: low component stresses, high frequency operation and soft-switching commutation. Converter design was done considering the operational constraints of the system MARK 1020.

A particular attention is done to the controller, which ensures a constant output voltage of the converter, in order to satisfy the requirements of the power system application and simultaneously keeps the PEM operating within its optimum operating point. The control implementation was divided into two parts namely: i) the voltage controller, which is responsible for keeping constant the output voltage of the converter even under loading variations and ii) the PEM controller, which is responsible for improving its performance by keeping the PEM fuel cell in its optimal operating point.

Due to significance of the PEM cell behavior the results are firstly presented for the PEM fuel cell model and then for the whole system with load.

The results demonstrate that the converter selected is a good solution to support the approach of improving the efficiency of PEM fuel cells because it allows an appropriated control of the power delivered by the fuel cell as it satisfies the requirements imposed by the load regulation with minimum of losses due to adoption of soft switching commutation.

Nomenclature

PEM – Proton exchange membrane fuel cell

IGBT – Insulated Gate Bipolar Transistor

SRC – Series resonant converter

ZVS – Zero voltage switching

ZCS – Zero current switching

A – Cell active area (cm2)

C – Equivalent electrical capacitance (F)

ENernst – Thermodynamic potential

Jmax – Maximum current density (A/cm2)

n – Number of cells in stack

PO2 – Oxygen partial pressure (atm)

PH2 – Hydrogen partial pressure (atm)

RC – Contact resistance (Ω)

RM – Equivalent membrane resistance (Ω)

T – Cell operating temperature (K)

Vact – Activation voltage drop (V)

Vohmic – Ohmic voltage drop (V)

Vcon – Concentration voltage (V)

ξi, ψ – Parametric coefficients

λ – Membrane thickness (μm)

fr – Resonant frequency (Hz)

wr – angular frequency (rad/s)

Zr – Resonant impedance (Ω)

Lr – Resonant tank inductor (H)

Cr – Resonant tank capacitor (F)

Q – Quality factor

Acknowledgements

Author details

Maria Teresa Outeiro[1*] and Adriano Carvalho[2]

*Address all correspondence to: touteiro@isec.pt

1 Department of Electrical Engineering, Institute of Engineering of Coimbra, Institute of Systems and Robotics – Porto, Portugal

2 Department of Electrical and Computer Engineering, University of Porto, Institute of Systems and Robotics – Porto, Portugal

References

[1] Corrêa, J.M., et al. An electrochemical-based fuel cell model suitable for electrical engineering automation approach. IEEE Transactions on Industrial Electronics, 2004; 5(51) 1103-1112.

[2] Yu, D. and S. Yuvarajan. A novel circuit model for pem fuel cells. Proceedings of IEEE Applied Power Electronics Conference and Exposition. 2004.

[3] Friede, W., S. Raël, and B. Davat. Mathematical model and characterization of the transient behavior of a PEM fuel cell. IEEE Transactions on Power Electronics 2004; 5(19) 1234-1241.

[4] Forrai, H., Yanagita Y., and Kato Y. Fuel-cell parameter estimation and diagnostics. IEEE Transactions on Energy Conversion 2005; 3(20): 668-675.

[5] Outeiro, M.T., et al., A Parameter Optimized Model of a PEM Fuel Cell Including Temperature Effects. Journal of Power Sources 2008; 185(2) 952-960.

[6] Outeiro, M.T., et al. Dynamic Modeling and Simulation of an Optimized Proton Exchange Membrane Fuel Cell System. Proceedings of International Mechanical Engineering Congress and Exposition. Seattle, USA. ASME; 2007.

[7] Kristina Haraldsson, K.W. Evaluating PEM fuel cell system models. Journal of Power Sources 2004; 126(1-2) 88-97.

[8] Bernardi, D.M. and Verbrugge M.W. A mathematical model of the solid-polymer-electrolyte fuel cell. Journal of Electrochemical Society 1992; 2477–2491.

[9] Rowe, A. and Li X. Mathematical modelling of proton exchange membrane fuel cells. Journal of Power Sources, 2001; 82-96.

[10] Mann, R.F., et al. Development and application of a generalised steady-state electrochemical model for a PEM fuel cell. Journal of Power Sources 2000; 173-180.

[11] Amphlett, J.C., et al. A model predicting transient responses of proton exchange membrane fuel cells. Journal of Power Sources 1996; 183-188.

[12] Wang, C. and Nehrir M. Dynamic models and model validation for PEM fuel cells using electrical circuits. IEEE Transactions on Energy Conversion 2005; 2(20) 442-451.

[13] Andersen, G.K., et al. A new power converter for fuel cells with high system efficiency. International. Journal of Electronics 2003; 90(11-12) 737-750.

[14] Xu, H., Kong L., and Wen X. Fuel Cell Power System and High Power DC–DC converter. IEEE Transactions on Power Electronics 2004; 19(5) 1250-1255.

[15] Shiju, W. Design and hardware implementation of a soft-switched converter for fuel cell applications. MsC thesis. University of Texas; 2006

[16] Krykunov, O. Comparison of the DC/DC-Converters for Fuel Cell Applications. International Journal of Electrical Computer and Systems Engineering 2007; 1(1) 71-79.

[17] Rathore, A., Bhat A., and Oruganti R. A Comparison of Soft-Switched DC-DC Converters for Fuel Cell to Utility Interface Application. IEEE Proceedings 2007; 588-594.

[18] Rong-Jong, W. and Rou-Yong D. High-Efficiency Bidirectional Converter for Power Sources With Great Voltage Diversity. IEEE Transactions on Power Electronics 2007; 22(5) 1986-1996.

[19] Ying-Chun Chuang, Y.-L.K., Hung-Shiang Chuang, Hung-Kun Chen Implementation and Analysis of an Improved Series-Loaded Resonant DC–DC Converter Operating Above Resonance for Battery Chargers. IEEE Transactions on Industry Applications 2009; 45(3) 1052 – 1059.

[20] Cancelliere P., et al. Modeling and Control of a Zero-Current-Switching DC/AC Current-Source Inverter. IEEE Transactions on Industrial Electronics 2007; 54(4) 2106-2119.

[21] Lee Y.-S., Chiu Y.-Y. and Cheng M.-W. Inverting ZCS Switched-Capacitor Bi-directional Converter, 37th IEEE Power Electronics Specialists Conference, Jeju, Korea, PESC; 2006.

[22] Yuang-Shung, L., et al. Multiple Output Zero-Current Switching Bi-directional Converter. 33rd Annual Conference of the IEEE Industrial Electronics Society, Taiwan Japan, IECON; 2007.

[23] Mohan N. and Underland T. Power Electronics Converters Applications and Design. John Wiley and Sons, Inc. 2003.

[24] Peng, F.Z., et al. A New ZVS Bidirectional DC–DC Converter for Fuel Cell and Battery Application. IEEE Transactions on Power Electronics 2004; 19(1) 54-65.

[25] Krykunov O. Comparison of the DC/DC-Converters for Fuel Cell Applications. International Journal of Electrical Computer and Systems Engineering 2007; 1(1) 71-79.

[26] Lee J.-Y., Jeong Y.-S. and Han B.-M. An Isolated DC/DC Converter Using High-Frequency Unregulated LLC Resonant Converter for Fuel Cell Applications. IEEE Transactions on Industrial Electronics 2011; 58(7) 2926 - 2934.

[27] Xin Kong, A.M.K., Analysis and Implementation of a High Efficiency Interleaved Current-Fed Full Bridge Converter for Fuel Cell System. IEEE Transactions on Power Electronics 2007; 22(2) 543-550.

[28] Averberg A., Meyer K.R. and Mertens A. Current-fed full bridge converter for fuel cell systems. IEEE Power Electronics Specialists Conference, Rhodes, Greece. PESC; 2008.

[29] Changchien S., Liang T., Chen J. and Yang L. Novel High Step-Up DC–DC Converter for Fuel Cell Energy Conversion System. IEEE Transactions on Industrial Electronics 2010; 57(6) 2007 – 2017.

[30] Blaabjerg F., Chen Z. and Kjaer S.B. Power Electronics as Efficient Interface in Dispersed Power Generation Systems. IEEE Transactions on Power Electronics 2004; 19(5) 1184-1194.